Earth Science Research; Vol. 6, No. 2; 2017
ISSN 1927-0542 E-ISSN 1927-0550
Published by Canadian Center of Science and Education

Tropical Moisture Exports, Extreme Precipitation and Floods in Northeastern US

Mengqian Lu[1,2] & Upmanu Lall[2,3]

[1] Department of Civil and Environmental Engineering, Hong Kong University of Science and Technology, Kowloon, Hong Kong SAR, China

[2] Columbia Water Center, Columbia University, New York, NY, USA

[3] Department of Earth and Environmental Engineering, Columbia University, New York, NY, USA

Correspondence: Mengqian Lu, Department of Civil and Environmental Engineering, Hong Kong University of Science and Technology, Kowloon, Hong Kong SAR, China。 E-mail: mengqian.lu@ust.hk

Received: April 6, 2017 Accepted: April 26, 2017 Online Published: June 28, 2017

doi:10.5539/esr.v6n2p91 URL: https://doi.org/10.5539/esr.v6n2p91

Abstract

A statistically and physically based framework is put forward to investigate the relationship between Tropical Moisture Exports (TMEs), extreme precipitation and floods in the Northeastern United States (NE-US). We found that the NE-US floods in the four seasons are closely related to TMEs and four major moisture sources of TMEs in the tropics account for approximately 85% of all the TMEs that enter the NE-US. The seasonality and interannual variation of the birth processes in the four source regions determine their contribution to the NE-US. Moisture born in Gulf of Mexico (GP) and Gulf stream (GS) are the year-around sources, with some winter contribution from Pineapple Express (PE) region, and West Pacific (WP) region contributes the least. The overall order of their contribution to NE-US is GP>GS>PE>WP. Seasonal association between TMEs birth and ENSO are also found. The seasonal and interannual variations in atmospheric circulation patterns also play an important role in determining the TMEs' entrance to NE-US. Strong influence of active TMEs periods on the occurrence of extreme rainfall is also identified. We show that the extreme daily precipitation events are dominated by extreme TMEs' entering the NE-US in every season.

Keywords: tropical moisture exports, extremes, Northeastern United States, moisture sources, atmospheric steering, seasonal and interannual variability

1. Introduction

Surface temperature gradients (Lorenz, 1984; Jain et al., 1999; Karamperidou et al., 2012) drive the large scale atmospheric circulation, and hence the meridional transport of moist air masses, primarily born in tropical oceanic areas, to higher latitudes, often manifested as localized threads of strong moist air fluxes. There are a number of studies focusing on 'Atmospheric Rivers' (ARs), a concept first introduced by (Zhu and Newell, 1994) who defined an atmospheric phenomenon that features a narrow corridor of concentrated moisture, enhanced and elated tropospheric water vapor transport that have a large hydrologic effect. Recent studies have linked Atmospheric Rivers (Zhu and Newell, 1998; Bao et al., 2006) to extreme precipitation and floods (Ralph et al., 2006; Leung and Qian, 2009; Lavers et al., 2011, 2013; Ralph and Dettinger, 2011; Lu et al., 2013; Lavers et al., 2016) as the major hydrometeorological contributor. ARs have been linked to extreme precipitation in the United Kingdom (Lavers et al., 2011, 2013; Nakamura et al., 2013), Western France (Lu et al., 2013), Midwest United States (Nakamura et al., 2013) and the West coast of United States (Ralph et al., 2006; Dettinger, 2011; Ryoo et al., 2011; Lavers et al., 2016) which has been linked to the well-known "Pineapple express" (Higgins et al., 2000), that originates from oceanic areas adjacent to Hawaiian Islands. However, areas such as the Northeastern United States (NE-US) have not been studied as much in this context. In a previous study for Western France (Lu et al., 2013), we saw moisture tracks for some extreme storms in France originating in the Gulf of Mexico and passing through NE-US, with precipitation in the NE-US enroute to France, and we also observed seasonally changing spatial patterns of the TMEs tracks entered this region. Thus, the NE-US was chosen in this study as a pilot to develop the statistical and physical based framework for hydrometeorological extremes with a focus on diagnosis of associated atmospheric circulation and climate teleconnection.

The widely used definition of ARs as a narrow plume with at least 2cm of integrated water vapor (IWV), extending over thousands of kilometers long and hundreds of kilometers wide (Ralph et al. 2004; Neiman et al. 2008; Dacre et al. 2015; Jeon et al. 2015), has restricted the studies to popular AR-associated regions as indicated in the preceding paragraph. In contrast, Bao et al. (2006) and Knippertz and Martin (2007), suggested the term "moist conveyor belt" to broaden the scope of the studies to Tropical Moisture Exports (TMEs) that may have significant contributions to hydrometeorological extremes on a global scale (Knippertz and Wernli, 2010; Knippertz et al., 2013; Nakamura et al., 2013; Lu et al., 2013). Here, we explore how TMEs may be involved in moisture transport into the NE-US, and how their sources and trajectories vary by season and under different ENSO regimes. The linkage of TMEs to extreme precipitation and flooding in each of the seasons is also assessed.

Past studies on the nexus of moisture transport, extreme precipitation and floods, focused on the (1) link to selected historical floods events in various regions (Ralph et al., 2006; Lavers et al., 2011; Lu et al., 2013; Nakamura et al., 2013); (2) identification of moisture sources that contribute to extremes (Knippertz and Wernli, 2010; Ryoo et al., 2011; Knippertz et al., 2013; Lu et al., 2013; Nakamura et al., 2013); and (3) trajectory analysis of the air masses with investigation of the attendant atmospheric circulation (Wernli, 1997; Bao et al., 2006; Ryoo et al., 2011; Nakamura et al., 2013; Lu et al., 2013). Lavers et al. (2011) linked ARs with the top 10 largest winter floods in Britain since 1970; while Nakamura et al. (2013) identified strong association between anomalous atmospheric circulations that drive low-level flow of warm and moist air, and 21 extreme floods in Ohio River. Further, Knippertz and Wernli (2010), Lu et al. (2013) and Nakamura et al. (2013) noted that the poleward transport of tropical born moist air masses to the Northern Hemispheric extratropics provide the link between tropical moisture sources and extratropical extreme precipitation, occasionally with explosive cyclogenesis. Lu et al. (2013) associated TMEs from the Gulf of Mexico and tropical North Atlantic Ocean as the major moisture sources for the 1995 January flood in western France, and demonstrated the predictability of the extreme precipitation given only the mid-latitude sea level pressure (SLP) fields, suggesting that steering mechanisms were important. A similar study for the extreme floods in Ohio River Basin by Nakamura et al. (2013) identified a persistent dipole pattern in the SLP leading to the wave like transport of moisture from the Gulf of Mexico into the flooded area, every 4 to 7 days over the March-April-May season. Further, Cioffi et al. (2015) identified the influence of North Atlantic Oscillation and El Niño Southern Oscillation (ENSO) on the changes of space-time structure of precipitation extremes in Europe over the last century.

1.1 Tropical Moisture Export Characterization

Tropical Moisture Exports (TMEs) were first documented in (*Knippertz and Wernli*, 2010) for Northern Hemisphere and later extended by *Knippertz et al.* (2013) to produce a global TMEs climatology. The TMEs tracks were calculated using 6-hourly ERA-Interim data (*Dee et al.*, 2011) and range from 1989 to 2010, covering daily tracks born in the tropics [0° – 20°N]. One-day forward tracks are calculated from every 100 km × 100 km × 30 hPa box between 0 and 20°N, between 1000 hPa and 490 hPa. Specific humidity can be converted into water mass as each track represents the same atmospheric mass of ~ 3×10^{12} kg *(Knippertz and Wernli 2010)*. Tracks are calculated with the LAGRANTO Lagrangian analysis tool (*Wernli*, 1997; *Wernli and Davies*, 1997), by interpolating the relevant fields to the positions of the track at the 6-hr updating frequency. To ensure that the moisture characteristics of the tropical air parcels are maintained on their way across the subtropics, only tracks that reach 35°N within the next 5 to 6 days after crossing 20°N were retained; however, changes due to fluxes of heat and moisture from the underlying surface or mixing cannot be completely excluded. The water vapor fluxes of the retained tracks in the dataset must reach 100 g kg^{-1} m s^{-1}, a threshold chosen to represent 'fast' events and yet get meaningful statistics (*Knippertz and Wernli*, 2010). *Knippertz and Wernli* (2010) showed that TMEs contributes significantly (more than 60% of the average) to climatological precipitation in the mid-latitudes and identified four major source regions in the tropics:

(1) "Pineapple Express' (PE) [170° – 130°W]. This source has a maximum activity in the December to Feburary (DJF) season and is almost absent ~~in~~ from June to Auguest (JJA).

(2) 'Great Plain' (GP) [100° – 90°W]. We extended this region to [100° – 70°W] from the *Knippertz and Wernli* (2010) after initial analyses revealed that it was the dominant source region for the TMEs entering the NE-US. This region includes the Gulf of Mexico, and also parts of the continental region between the Rocky and the Appalachian Mountains.

(3) 'Gulf Stream' (GS) [40° – 70°W]. This source is active year around with low seasonality.

(4) 'West Pacific' (WP) [120° – 170°E]. Although this source contributes the least, it is included in the analysis considering its correlation with the other three.

Subsequently, we identify the TMEs tracks as PE, GP, GS or WP as associated with their birthplace. The source

regions are marked in Figure 7 & 8.

The conceptual framework of the analysis presented in this paper is indicated in Figure 1. The causal structure illustrated considers the potential dependence of the TMEs birth process as a function of the source location, the season and ENSO state (this level of relationships is marked as red arrows in Figure 1). The birth process here refers to where and how many tracks are born and how these vary by season. The number of TMEs entering the NE-US on any given day depends on the associated birth process, the season, the source, the ENSO state, and the atmospheric circulation (this level is marked as blue arrows in Figure 1). The total water released (ΔQ) by the TMEs in the NE-US on a given day is taken to depend on the number of TMEs' entering. The extreme precipitation amount, EP, is considered to depend on the ΔQ (black arrows in Figure 1).

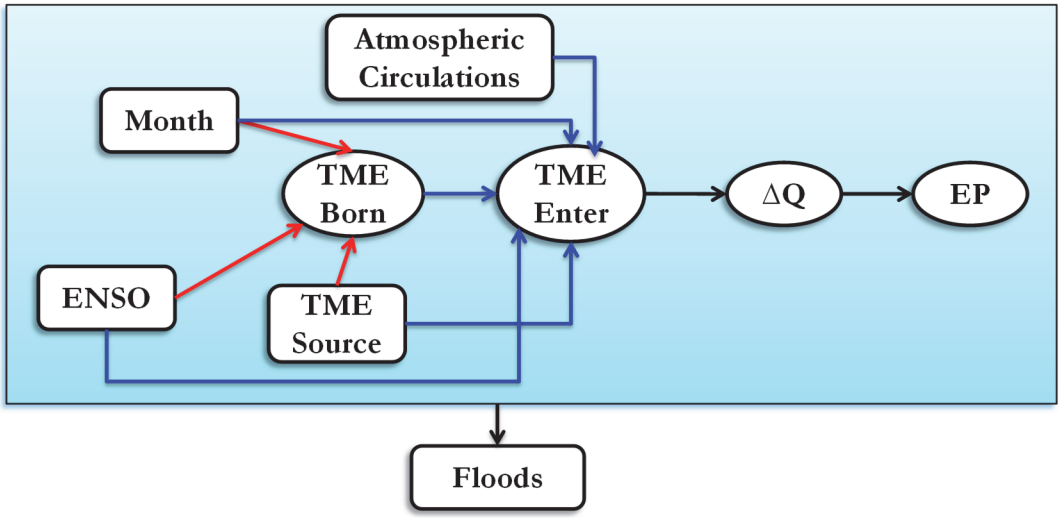

Figure 1. Influence diagram of the factors considered and their proposed relationship (as the arrows directed) investigated in this paper. EP is extreme precipitation, ΔQ represents moisture release from the TMEs tracks

We take the NE-US [39°N – 48°N, 66°W – 82°W] as the pilot study area to address the following questions and develop the framework that can be extended to other areas:

(1) How were floods events in NE-US in different seasons related to TMEs in terms of the moisture sources, the trajectories and their seasonality?

(2) What is the connection between the birth process of TMEs and the role of large scale climate regulation, e.g. ENSO?

(3) What is the relationship between the entrance of TMEs to NE-US and the role of atmospheric circulation patterns?

(4) What is the link between TMEs and extreme precipitation events that may trigger floods?

The paper is organized in line with answering these research questions. The data used in this study is provided in Section 2. In Section 3, we illustrate the association of TMEs with examples of extreme floods in each season. The second research question is addressed in Section 4. The entrance of TMEs to the NE-US and the associated atmospheric steering is discussed in Section 5. The link between moisture release and extreme precipitation that is closely related to floods is explored in Section 6. A discussion and summary of the key findings is provided in Section 7.

2. Data

The results of this study mainly use the TMEs dataset documented in (*Knippertz and Wernli*, 2010). The dataset covers from 1989 to 2010, recording daily tracks born in the tropics that meet the following criteria: (1) they reach 35°N within the next 5 to 6 days after crossing 20°N, and (2) water vapor flux of any track is not less than 100 g kg^{-1} m s^{-1}. For all TME trajectories, position information (longitude and latitude) is available every 6 hours, and up to 7 days.

We calculate the change of moisture (recharge or release) along each track as

$$\Delta Q_k(j) = Q_k(j) - Q_k(j+1) \quad (1)$$

where j is the time point on the track (the j^{th} position along the track), $Q_k(j)$ is the k^{th} TMEs track's specific humidity in g kg^{-1} (units) at time point j and $\Delta Q_k(j)$ is the change of specific humidity. Each of the tracks has its positions recorded every 6 hours, up to 7 days, with a total of 29 time points. Thus, j ranges from 0 to 28, with the birth location at $j = 0$ and the point before death location at $j = 28$.

The total release of water from the air parcel in the study area was calculated as the change of total specific humidify (including liquid phase) integrated over all the tracks for a given date starting from their entrance as follows:

$$\Delta Q(t) = \sum_{k=1}^{N_t}(Q_k(t) - Q_k(t+1)) \quad (2)$$

where $\Delta Q(t)$ is the total change of specific humidity of all the tracks that are active in the NE-US on day t, N_t is the total number of tracks active in the NE-US on day t. Note that we consider the tracks leaving/exiting at the different hours of the day, i.e. 0 o'clock, 6 o'clock, 12 o'clock, 18 o'clock, 24 o'clock. By examining the selected tracks and their release of moisture to the study area, the associated moisture birth location and their trajectories to the NE-US can be identified and the precipitation resulted from the release of water vapor from the moist air parcel can also be computed.

For the analysis of atmospheric circulation patterns, we choose the sea level pressure (SLP) data from the NCEP/NCAR Reanalysis project (*Kalnay et al.*, 1996) provided by the NOAA/OAR/ESRL PSD, Boulder, Colorado, USA at http://www.esrl.noaa.gov/psd/. We use the daily SLP data, with a resolution of 2.5° latitude× 2.5° longitude, covering the same period as the TMEs dataset, 1989 – 2010. We further derived the daily SLP anomalies against calendar day climatology as calculated as follows.

$$SLPa_{ij} = SLP_{ij} - SLPc_i \text{ where } SLPc_i = \frac{\sum_{j=1989}^{2010} SLP_{ij}}{22} \quad (3)$$

where i is the i^{th} day in year j, i = 1, …, 365 (366 for leap years) and j = 1989, …, 2010; $SLPa_{ij}$ is the SLP anomaly on i^{th} day in year j, $SLPc_i$ is the calendar day climatology of SLP on the i^{th} day of a year.

The Oceanic Niño Index (ONI) is provided by NOAA/National Weather Service, NOAA Center for Weather and Climate Prediction, Climate Prediction Center at http://www.cpc.ncep.noaa.gov/. The ONI has become the de-facto standard that NOAA uses for identifying El Niño (warm) and La Niña (cool) events in the tropical Pacific. The warm and cold episodes are based on a threshold of ± 0.5ºC of the running 3-month mean of ERSSTv3b data (*Smith et al.*, 2008) SST anomaly for the Niño 3.4 region (5°N – 5°S, 120° – 170°W). Cold and warm episodes are defined when the threshold is met for a minimum of 5 consecutive over-lapping seasons.

The flood events in NE-US we discuss in the following section are recorded by the Dartmouth Flood Observatory (DFO, at their website: http://floodobservatory.colorado.edu/). The Dartmouth Flood Observatory Achieve contains global floods events from 1985 to present based on data acquired by NASA, the Japanese Space Agency and the European Space Agency.

3. TMEs and Floods in the NE-US

For each of the four seasons, i.e., Dec – Jan – Feb (DJF), Mar – Apr – May (MAM), Jun – Jul – Aug (JJA) and Sep – Oct – Nov (SON), major flood events in the NE-US as recorded in the DFO data base were identified. For each event, TMEs tracks that were born in any of the four major source regions, listed in Section 1.1, and within 7 days of the onset of heavy precipitation in the flooded region were identified. Of these, those that entered the NE-US, including those that continued out of the region, were further identified. This two-step identification procedure yields a list of TMEs tracks that both were from the major source regions and contributed to the precipitation leading to the target flood events: a representative flood event is identified for each season and the TMEs tracks associated with it are shown in Figure 2. The colors indicate the changes of specific humidity along the tracks, calculated as in Eq. 1. Moisture release is recorded as blue or light blue dots in Figure 2, while moisture recharge magnitude is shown as red or yellow dots. Basic attributes of the exemplified flood events are summarized in Table 1. Enlarged panels of Figure 2 are attached in Appendix A for reference.

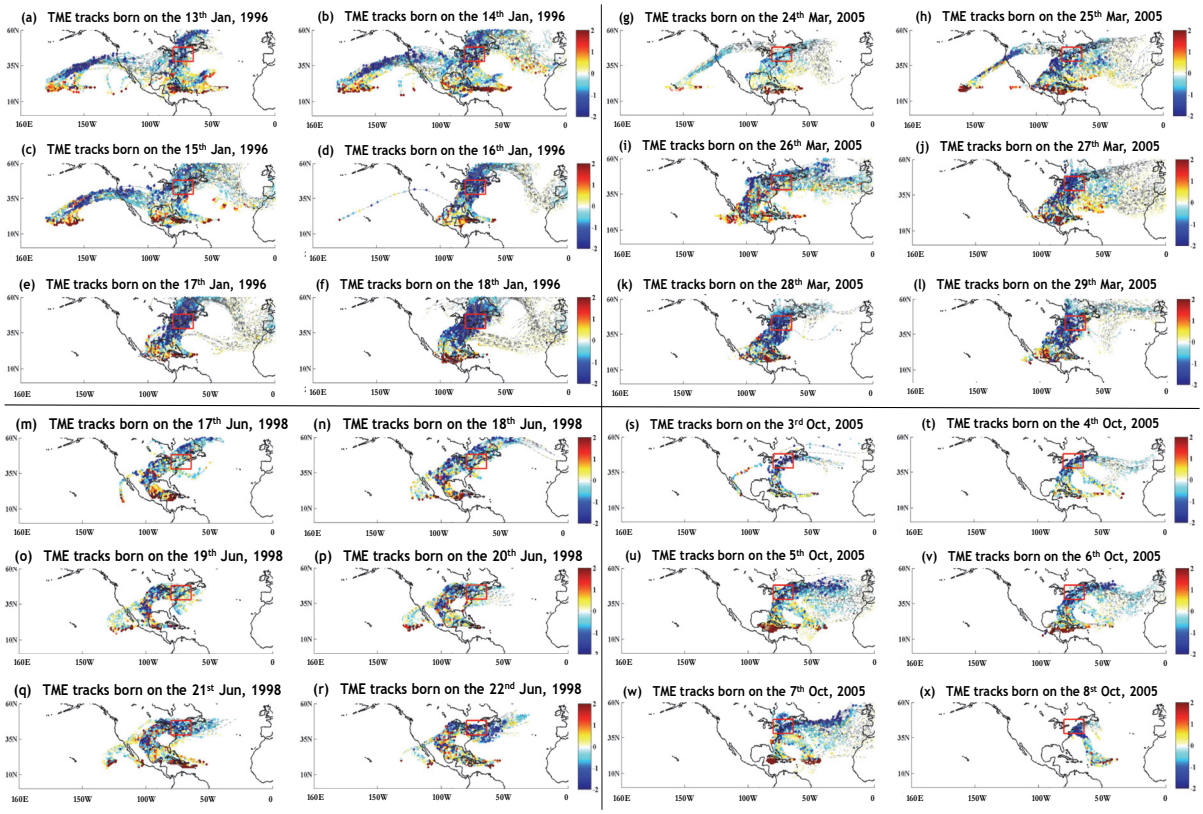

Figure 2. (a) – (f): DJF Flood: TMEs tracks that born between the 13th and the 18th Jan in 1996, when two successive flood events occurred, one started on the 15th in New York, Pennsylvania, Ohio, West Virginia, New Jersey; the other started 4 days later in Chateauguay, Quebec. (g) – (l): MAM flood: TMEs tracks that born between the 24th and the 29th Mar in 2005; broad area including New York, New Jersey, Delaware had flood started on the 1st of April. (m) – (r): JJA flood: TMEs tracks that born between the 17th and the 22nd Jul in 1998; heavy rainfall induced flood event in Green Mountain to Bradford, Vermont and New Hampshire. (s) – (x) SON flood: TMEs tracks that born between the 3rd and 8th Oct in 2005 associated with 10 days flooding from the 8th to the 17th of Oct in Southwest New Hampshire, Vermont, New Jersey and Connecticut. The red box highlights the NE-US with color indicating the changes of moisture from the tracks: red = recharge, blue= release; each dot corresponds to a 6-hour update of the air parcel position, i.e., trajectory of the tracks. Enlarged panels are provided in the Appendix A. The unit of the color bar is g kg^{-1}. (Dartmouth Flood Observatory Archive http://floodobservatory.colorado.edu/)

Table 1. Facts of the example flood events in the each of the four seasons, records are from Dartmouth Flood Observatory Archive

Season	DJF	MAM	JJA	SON
Location	US: New York, Pennsylvania, Ohio, West Virginia, New Jersey; Canada: Chateauguay, Quebec	New York, New Jersey, Delaware River	Green Mountain to Bradford, Vermont and New Hampshire, Mad River, White River and Ayers Brook	Southwest New Hampshire, Vermont, New Jersey, Connecticut
Time	1996, January	2005, April	1998, June	2005, October
Facts of the Floods	2 successive flood events occurred in NE-US and Quebec Canada, triggered by heavy rain and rapid snowmelt with anomalous warmer temperature	7 inches rainfall total with antecedent wet condition from Tropical Storm 'Ivan', worst flood event in the 50 years	8 inches rainfall total, flows exceeded the 100-year flood	12 inches of rainfall total, intensive rainfall of 7 inches within 30 hours period, flows exceeded the estimated 500-yr flood
Moisture Sources	GP, GS and PE	GP, GS, very few PE	GP, GS, few from East Pacific	GP and GS

Figure 2 (a) – (f) shows that the associated TMEs for the January 1996 flood (Table 1) were born in (1) 'Pineapple Express' (PE), i.e. Niño 3.4 region near Hawaii; (2) 'Great Plain' (GP), i.e. Gulf of Mexico and (3) 'Gulf Stream,' (GS), i.e. tropical North Atlantic ocean east to the Bahamas. The beginning of the heavy rainfall appears related to tracks born in all the three regions as shown in Figure 2 (a) – (c). Later in the event (Figure 2 (d) – (f)) TMEs that entered the NE-US were all born in GP and GS. The change of moisture content of the tracks indicates that for tracks born in PE, the relatively longer travel time and distance resulted in more recharging and releasing on their way to the NE-US, compared to GP and GS, which featured less changes of moisture content before reaching the flooded area, and relatively more release in the NE-US (more dark blue dots of tracks in Figure 2 (d) – (f) in the red box – NE-US). There are strong spatial patterns of the trajectories given the TMEs tracks' sources: tracks from PE follow typical northeastwardly 'Pineapple Express' sine-wave like trajectory showed in the AR literature focusing on the west coast [e.g., (Dettinger, 2011; Dettinger et al., 2011; Ralph and Dettinger, 2011)]; tracks from GP and GS penetrated to the north until reaching 50°N, where the jet stream locates, and then turned to the east. Lu et al. (2013) showed remarkably similar trajectories of the two major sources, i.e. GP and GS, associated with the more than 100-yr heavy precipitation induced flood event in Western France in January 1995. It suggested that moist air parcels originated from the tropics can have far impacts on extremes in the higher latitudes; and floods occurred at different time and over different regions may share the same moisture sources in terms of the TMEs.

The major moisture sources identified for the April 2005 event (Figure 2 (g) – (l)) are GP and GS. There were a few TMEs tracks from PE, which contributed only to the early stage of the heavy rainfall, indicated by both the number of tracks and moisture release. It took averagely 6 – 7 days, depending on the carrying wind speed and season, for TMEs tracks born in PE to reach the NE-US. The major contributors are thus GP and GS, which are both very active in MAM (Knippertz and Wernli, 2010). The PE TMEs (Figure 2 (g) – (h)) propagated further north reaching 50°N, different from the winter event shown in Figure 2 (a) – (f). The same is the case for the TMEs born in GP and GS (Figure 2 (g) – (l)). This may be associated with the beginning of the seasonal northward shift of the jet stream (Laing and Michael Fritsch, 1997). The moisture released from the TMEs was a significant fraction of the moisture carried by the tracks, and Figure 2 (h), (j) – (l) show that the most extensive releases were occurred in the NE-US.

The major moisture sources associated with exemplified summer flood in June 1998 are GP and GS, with some from the tropical East Pacific. The most notable feature in Figure 2 (m) – (r) is the well-organized spatial trajectory of all TMEs tracks that bring moisture from the warmer tropical ocean to the Great Plains, starting to release moisture in the Mississippi river basin before reaching NE-US. A flood event in Southwest Iowa occurred right before this NE-US flood, which agrees with the observation that the TMEs (Figure 2 (m) – (r)) followed the path passing both of the flooded regions in a consistent order. Note that only TMEs tracks that finally entered NE-US have been retained in Figure 2 (m) – (r), and there were additional TMEs tracks that were responsible for the Southwest Iowa floods but they did not eventually reach the NE-US. Due to the longer distance of these trajectories and the weaker westerly in summer, it took longer for the TMEs to reach NE-US after they were born. The trajectories of TMEs exiting the NE-US were different in Figure 2 (m) & (n) and Figure 2 (q) & (r). The TMEs in (Figure 2 (m) & (n)) went further north to Quebec, Canada; while the ones born on the 21st and 22nd (Figure 2 (q) & (r)) followed a wavelike trajectory starting from the Great Lakes. The changing trajectories were likely associated with synoptic scale transients (Lu et al., 2013).

Figure 2 (s) – (x) shows the TMEs tracks that contributed to the October 2005 flood event (Table 1). The major moisture sources identified are GP and GS. The most notable feature in Figure 2 (s) – (x) is the similarity to the trajectories of those born in GS in DJF (Figure 2 (a) – (f)). TMEs born in GS remained in the oceanic sector before reaching the NE-US, which resulted in a continuous recharging of moisture to the tracks. At the same time in October 2005, it was reported that remnants of Tropical Storm Tammy and Subtropical Depression Twenty-two merged with incoming continental cold fronts to produce torrential rains over the NE-US. The trajectories of the GS TMEs are consistent with these storms. Such a feature is not typically consistent with ARs. The release of the moisture was concentrated in the NE-US.

The four flood event examples show that in the NE-US, TMEs may be closely related to floods year-around with varying major moisture sources and trajectories. The main year-around moisture sources shown in these four events are GP and GS with some contributions from PE in DJF.

4. TMEs Birth and ENSO

In each season, TMEs from different moisture sources were seen to be associated with floods in the NE-US. Cioffi et al. (2015) also linked NAO and ENSO to the space-time structure of precipitation extremes in Europe

and its changes, based on the data over the past century. Cioffi et al. (2015) also encouraged a further study on the influence of ENSO on extremes, together with its modulation of the atmospheric circulation. Thus, the seasonality of and interannual variations in TMEs birth and its association with ENSO are analyzed in this section. Figure 3 presents the seasonality of and the interannual variations in the TMEs born in the four major sources under different ENSO phases. All four sources show a strong seasonality of the TMEs birth process.

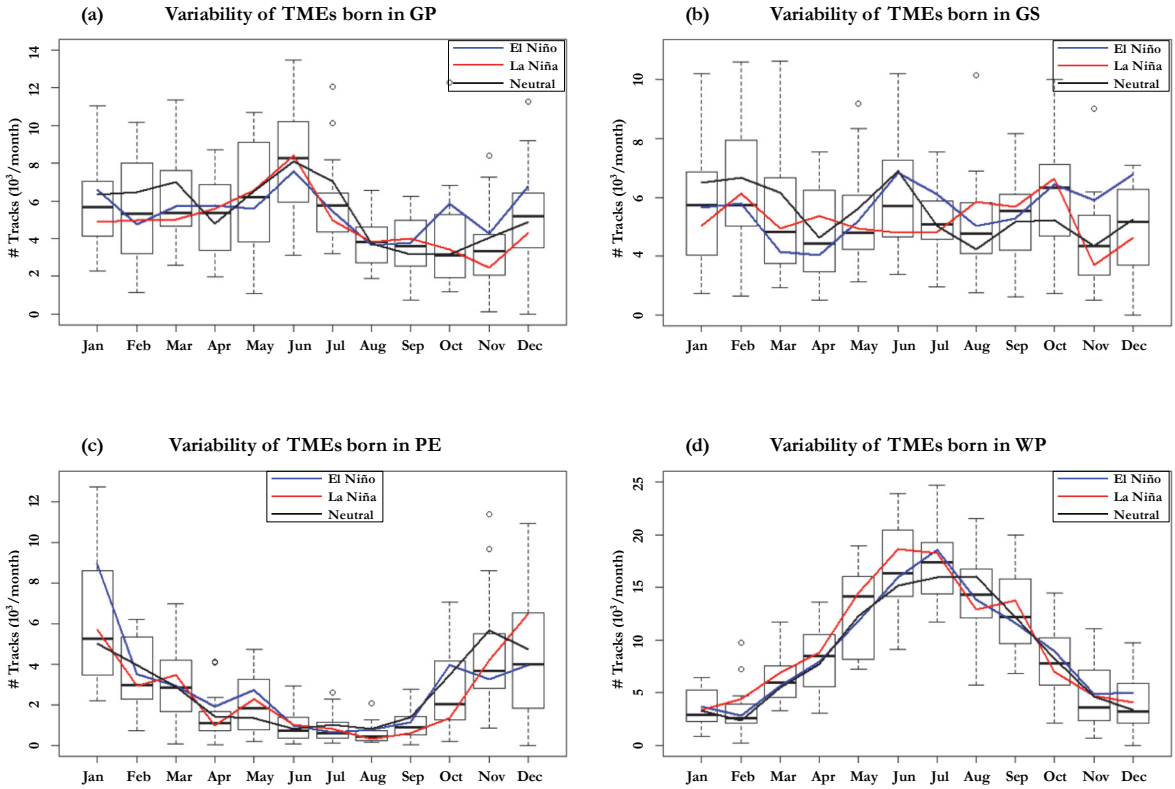

Figure 3. Seasonality and interannual variations of the monthly total number of TMEs born in the four major source regions (a) GP, (b) GS, (c) PE and (d) WP and the influence of ENSO scenarios on their monthly average amounts: blue is the composite of the El Niño years; red is the composite of the La Niña years; black is the composite of the neutral years

GP is active year-around and peaks in June (Figure 3 (a)). The largest divergence between El Niño and La Niña conditions occurs in Oct – Jan, with enhanced TMEs under El Niño and suppressed TMEs under La Niña conditions. A t-test for the difference in mean GP TMEs counts, for those born in Oct – Jan, considering unequal variance in each phase, i.e., El Niño and La Niña phases, yields a p-value of 0.008 for the null hypothesis of no difference.

GS (Figure 3 (b)) is relatively less active than GP, and has a weaker seasonality with multiple peaks in DJF, June and October. The largest divergence between El Niño and La Niña phases occurs in Nov – Dec (p level from the t-test is 0.048), and June – July (p level from the t-test is 0.013) when TMEs are enhanced in the El Niño phase, and in Mar – April (p level from the t-test is 0.050) when TMEs are enhanced in the La Niña phase (Figure 3 (b)). It is interesting that TMEs are suppressed in both El Niño and La Niña phases relative to the neutral phase in JFM, and enhanced in Aug – Oct.

PE (Figure 3 (c)) and WP (Figure 3 (d)) have very strong seasonality, evidenced by their large variances of TMEs born in different months. The two have opposite peaking seasons: WP (Figure 3 (d)) is very active in summer, when it is the monsoon season for East Asia. PE (Figure 3 (c)) is active in winter, when the 'Pineapple Express' ARs are the most active and affect the west coast of the United States. There is a persistent increase in WP TMEs (Figure 3 (d)) in Feb – Jul (p level from the t-test is 0.09) in the La Niña phase. For PE (Figure 3 (c)), the situation is mixed, with enhancement under El Niño in January and October (p level from the t-test is 0.06), but under La Niña in December as the largest divergence.

5. TMEs entrance and Atmospheric Circulation Patterns

The origins of the TMEs entering NE-US vary seasonally, due in part to the seasonality of the TMEs birth, and in part to the seasonal and interannual variations in atmospheric circulation patterns. The conditional probability P(Source|NE) that the TMEs that entered the NE in a given month comes from a particular source, and its interannual variation are illustrated in Figure 4. The calculation of conditional probability in this study followed the classic ratio analysis. The corresponding data for the total number of tracks entering by calendar month, the total number of tracks from the four sources considered here, and the annual total for each source are supplemented and presented in the Appendix B Table B.2.

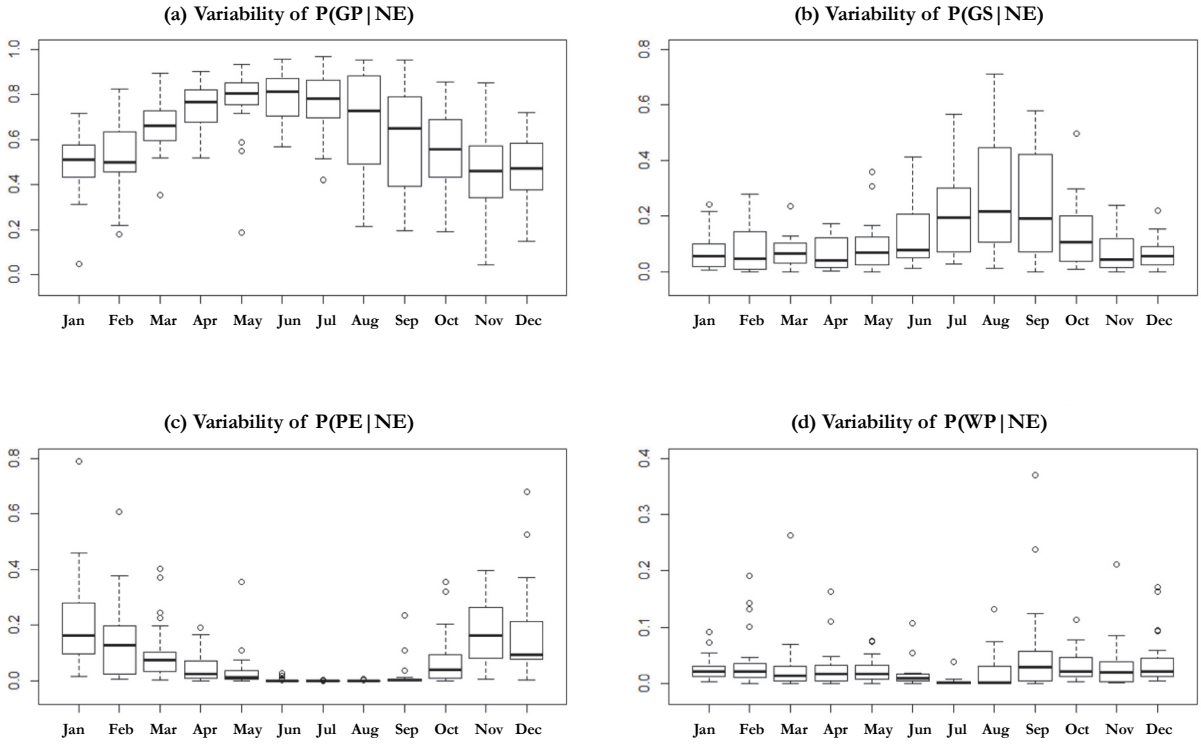

Figure 4. Boxplots of the conditional probabilities of TMEs birthplace (sources regions), given TMEs tracks entered NE-US showing the seasonal and interannual variability of contributions of TMEs tracks from (a) GP, (b) GS, (c) PE and (d) WP

First, we note that the four sources considered account for 85% of all tracks entering the NE-US on an annual average basis, varying cyclically from a minimum of 70% in December to a maximum of 98% in July (Table B.2). The number of TMEs tracks entering peaks in the winter with a secondary maximum in June. On an annual basis, approximately 73% of the tracks come from GP, 14% from GS, 11% from PE and 3% from WP. Consequently, it is not a surprise that on average, 45% (Nov) to 79% (June) of the tracks on a monthly basis come from GP. The fraction coming from GS increases from June to October and peaks in August (28%). PE's contributions are important in November to February (~20% of the tracks), and WP is a weak spring/fall contributor accounting for a maximum of 4% of the tracks in December and February. In summary, GP is important year around, but particularly in April – July, GS has increased contributions in June – October, and PE in November – February, with WP a possible contributor in winter.

From Figure 4, we see that GP accounts for a relatively stable seasonality of tracks entering across the year, with a consistent peak in June (~80%), and minimum in Nov – Feb (~45%) and high interannual variability in August, September and November. GS is an important source in July – September with high interannual variability. PE is primarily a contributor in Nov – Feb, while WP has a low contribution throughout the year with relatively high variability across years in fall and spring.

Tracks entering from GP into the NE-US are positively correlated at a significance level of 0.05, with those entering from GS in January (correlation=0.62), February (0.79), March (0.71), September (0.37), November (0.51) and December (0.68); with PE tracks entering in November (0.37) and December (0.18), and with WP

tracks in January (0.52) and February (0.39). Tracks entering from GS and PE are negatively correlated in January (-0.32) and October (-0.38). Tracks entering from PE and WP are positively correlated in December (0.26).

The seasonal and interannual variability in the relative contributions of the tracks from different sources may be due to changes in the TMEs birth or TMEs steering characteristics. To develop some understanding of these issues, the statistics of TMEs birth and the conditional probability of tracks born in a region entering the North East, P(NE|Source) are illustrated in Figure 5 and supplemented in Appendix B Table B.2.

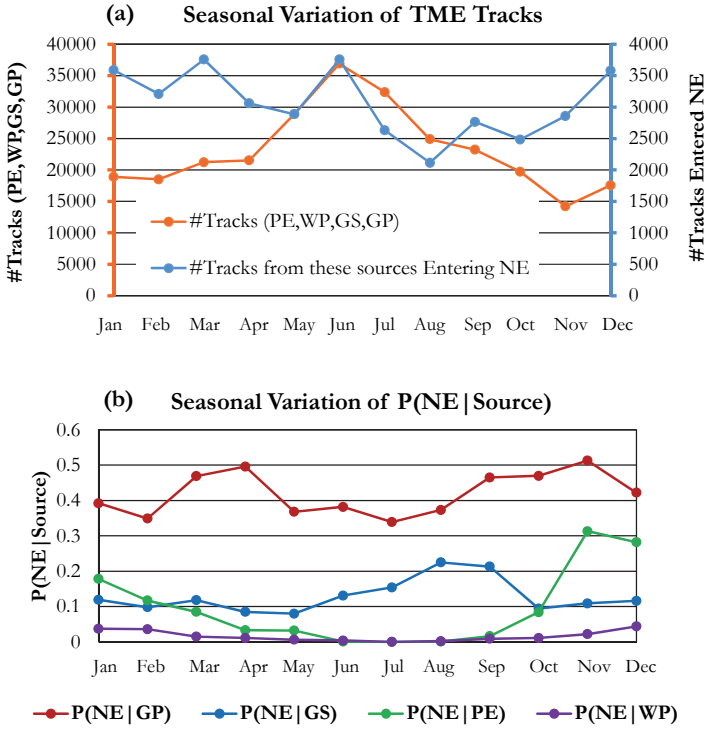

Figure 5. (a) Seasonal variation of the TMEs born in the four major sources and the seasonally varying portions of these TMEs entering NE-US, note that the TMEs born refer to the y-axis on the left and entrance refer to the y-axis on the right, whose scale is 1/10 of the left; (b) seasonal variation of the probability of TMEs entering NE-US given TMEs born in four major source regions

First, we note that the total tracks born aggregated across the four source regions have a pronounced seasonality with a maximum in March, June and December and a minimum in August (Figure 5(a) & Table B.2). In terms of the proportion of tracks born in the four source regions that essentially entered NE-US, on average only 13% of these tracks enter the NE-US, with a minimum of 8% in August, a maximum of 20% in November and December and an active 18% in JFM. Consequently, the seasonal cycle of the tracks entering the NE-US has a minimum in August, with peaks in December to March and in June.

On average, 42% of the GP TMEs enter NE-US with small variation from month to month, slightly lower in May-August, and higher in March-April and September to December (Figure 5(b) & Table B.3). The GP birth, i.e. P(GP) (Figure 3 (a)), varies across the year with a peak in June, while its entrance, i.e. P(NE|GP) (Figure 6 (a)), undergoes small changes through the year but has strong interannual variations in January and October. A t-test for the difference in mean GP TMEs entrance counts considering unequal variance in each phase, i.e., El Niño and La Niña phases, yields no difference. Therefore, the variations in the birth process of GP tracks over the year dominate the contributions to the seasonality of the TMEs that enter the NE-US.

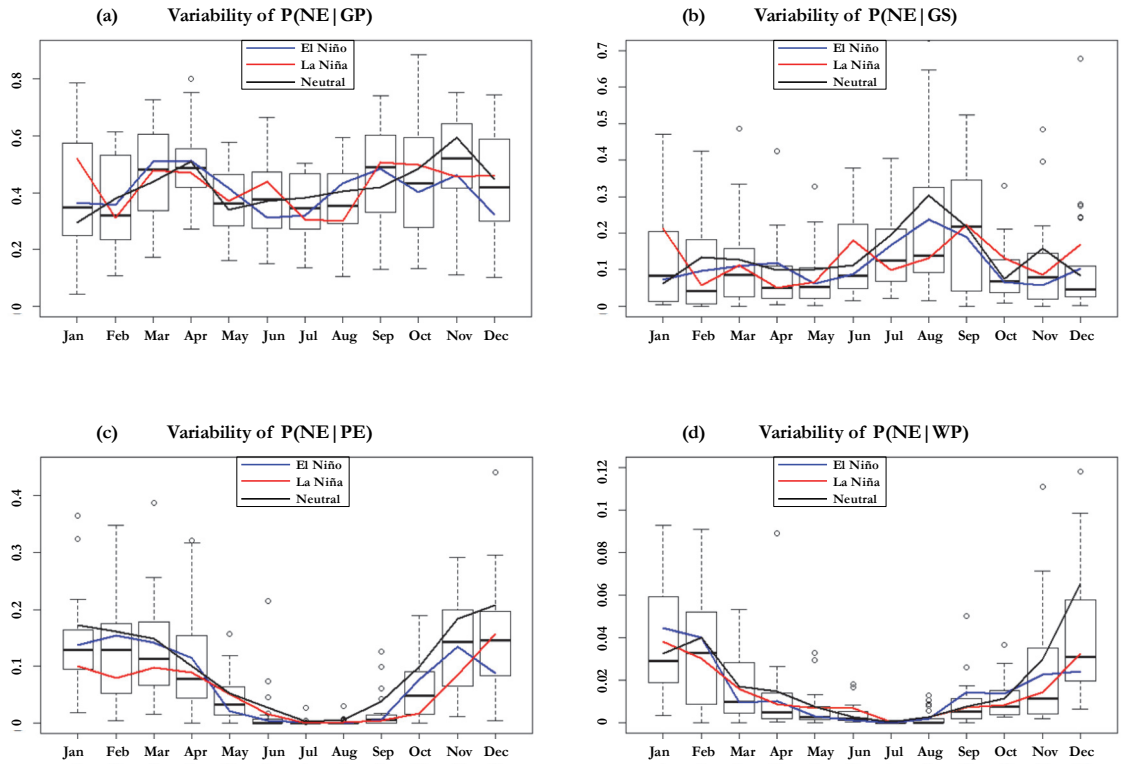

Figure 6. Seasonality and interannual variations of the conditional probabilities of TMEs Entrance to NE-US for each month, given TMEs born in the four major source regions in the tropics: (a) GP, (b) GS, (c) PE and (d) WP; and the influence of ENSO episodes: blue is the composite of the El Niño years; red is the composite of the La Niña years; black is the composite of the neutral years

GS TMEs entering NE-US accounts for 13% of the tracks born with variations from 8% in May to 23% in August (Figure 5(b) & Table B.2). GS TMEs entrance is active in June through September, while P(NE|GS) peaks at the same period during El Niño phase and neutral phase of ENSO (Figure 6 (b)), with anomalous decreases in July and August in La Niña phases. While the GS birth (Figure 3 (b)) has multiple peaks in DJF, June and October, the June peak is suppressed in the La Niña phase relative to the Neutral and El Niño phases. December GS birth is enhanced during El Niño phase, while January and February are suppressed during both El Niño and La Niña years. In La Niña years, the GS birth drops in June, July (GS entrance also drops in La Niña in July (Figure 6 (b)), November with two mild peaks in October and February. Thus, it appears that ENSO may influence the birth process more than the steering process for GS TMEs tracks coming to the NE-US.

PE TMEs begins its entrance in October until March (Figure 5(b)) with its peak contribution in November (31%) and December (28%) (Table B.2). PE birth is active at the same time period with strong interannual variations. In La Niña years, there is a decrease of P(NE|PE) in October to March, while it is also suppressed in the El Niño years in Oct – Dec (Figure 6 (c)).

WP TMEs entrance is the least of the four sources through the year (Figure 5(b)), though its birth peaks from May to September (Figure 3(d)). P(NE|WP) is low and the separation by ENSO episodes is minor.

In summary, it appears that ENSO's dominant influence on the interannual variations in the birth process for GP and GS, and on the steering and birth process for PE. The expression of the ENSO influence varies by time of year in both birth and steering. Interannual variability in P(NE|GP) is highest in May – June, but does not appear to be related to ENSO. The variability in P(NE|GS) is highest for August – September, and again does not have a clear ENSO influence. For P(NE|PE) the Oct – March period is the most active and does seem to be influenced by ENSO.

Figure 7 and Figure 8 provide the composites of daily sea level pressure anomalies of the top 10% TMEs active entrance days and the top 10% TMEs inactive entrance days on a monthly basis to illustrate the differences of the atmospheric circulation patterns associated with the activity of TMEs' entrance. We consider the total number of TMEs that from all sources including regions that outside the four major sources. The top 10% TMEs active

days are determined by the total number of TMEs entering NE-US by finding the days that have TMEs exceeds the 90% percentile of the daily TMEs tracks for that month over the 22 years (1989 – 2010). The top 10% TMEs inactive entering days are determined by finding the days that have TMEs below the 10% percentile of the daily TMEs tracks for that month over the 22 years. To assist the comparison of the associated circulation patterns, we have corresponding active and inactive composites side by side (left panel: active TMEs entrance; right panel: inactive TMEs entrance) for each month (Jan – Jun in Figure 7 and Jul – Dec in Figure 8). Winter (DJF) active TMEs entrance is observed to be associated with low-wavenumber SLPa patterns around 60ºN; spring (MAM) active TMEs are associated with lows in the Great Plain east to the Rocky Mountains; summer (JJA) TMEs entrance has less association with large circulation patterns; Fall (SON) TMEs active entrance days are associated with lows in Great Plains; its inactive entrance associated with high-wavenumber blocks in the mid-latitudes in November (Figure 8(k)). Figure 7 and 8 link the large scale atmospheric circulation with TME entrance. They compare the composite anomalies between active and inactive TME entrance days. For the TME to enter the study area, the associated atmospheric circulation pattern has to be in favour of such convergence of moist air, and we think the large-scale organization contributes to the local organization as shown in our previous study (Lu et al. 2013) in Western France, and it also relates to the wave interaction hypothesis advanced in (Screen and Simmonds 2014).

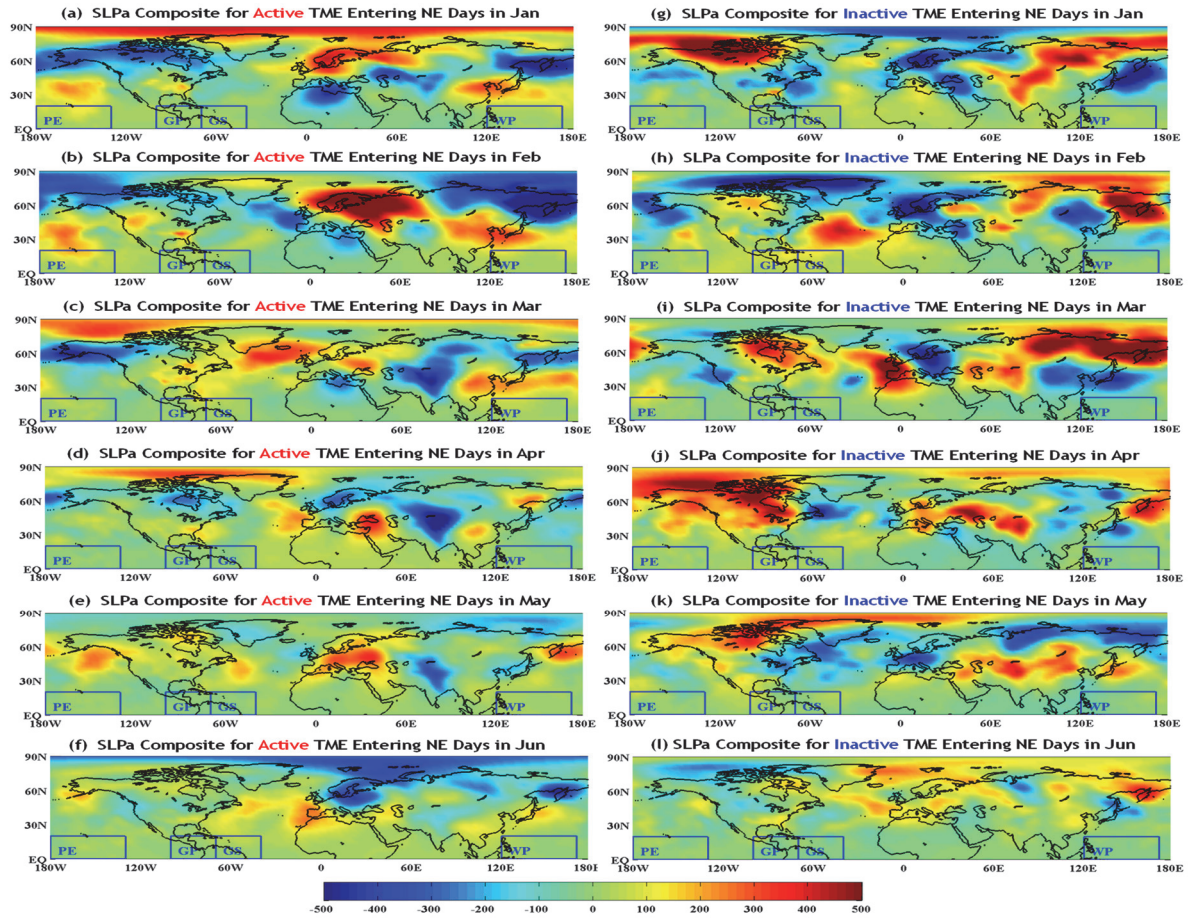

Figure 7. Composite of daily Sea Level Pressure anomalies of the top 10% TMEs active entering NE-US days in each month from January to June ((a) – (f)), over the 22 years (1989 -2010); and composite of daily Sea Level Pressure anomalies of the top 10% TMEs inactive days in each month from January to June, (g) – (l), over the 22 years (1989 -2010). TMEs active entering days are categorized as the days which have the number of total TMEs tracks entering NE-US exceeding its monthly 90% percentile; the composite is done for each month, with 90% percentiles calculated for each month over the 22 years; TMEs Inactive entering days are categorized as the days which have the number of total TMEs tracks entering NE-US below its monthly 10% percentile; the composite is done for each month, with 10% percentiles calculated for each month over the 22 years; the four major TMEs sources in the tropics are marked in blue rectangular boxes with their names: PE (Pineapple Express), GP(Great Plains), GS(Gulf Stream) and WP (West Pacific). Unit of the color bar is hPa.

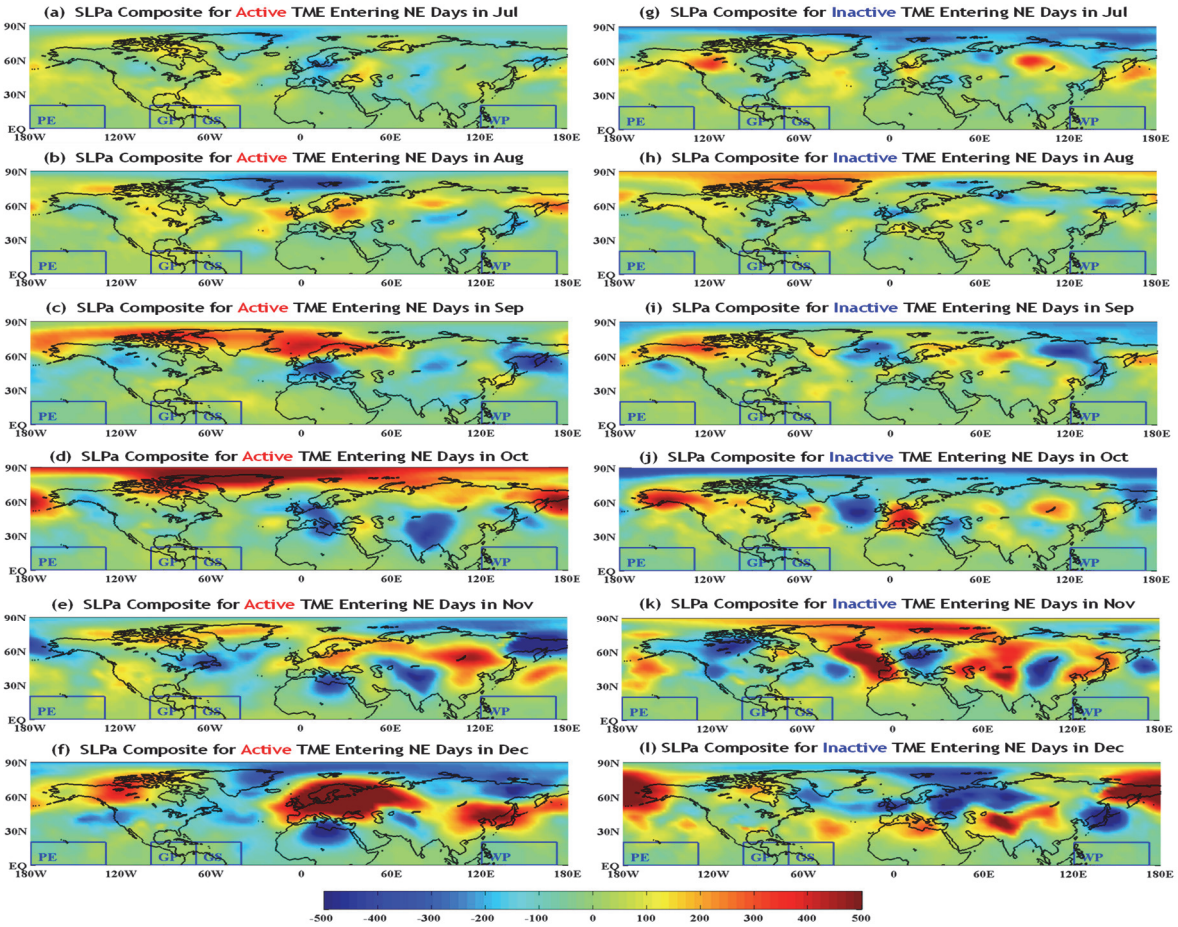

Figure 8. Composite of daily Sea Level Pressure anomalies of the top 10% TMEs active entering NE-US days in each month from July to December ((a) – (f)), over the 22 years (1989 -2010); and composite of daily Sea Level Pressure anomalies of the top 10% TMEs inactive days in each month from July to December, (g) – (l), over the 22 years (1989 -2010). TMEs active entering days are categorized as the days which have the number of total TMEs tracks entering NE-US exceeding its monthly 90% percentile; the composite is done for each month, with 90% percentiles calculated for each month over the 22 years; TMEs Inactive entering days are categorized as the days which have the number of total TMEs tracks entering NE-US below its monthly 10% percentile; the composite is done for each month, with 10% percentiles calculated for each month over the 22 years; the four major TMEs sources in the tropics are marked in blue rectangular boxes with their names: PE (Pineapple Express), GP(Great Plains), GS(Gulf Stream) and WP (West Pacific). Unit of the color bar is hPa.

6. TMEs and Extreme Precipitation

The moisture release from the tracks in NE-US is highly correlated with the total number of TMEs entering NE-US (concurrent correlation between number of TMEs entering and ΔQ in NE-US is 0.88 (p-value < 10-4). We estimated the conditional density of daily precipitation given total daily change of specific humidity (ΔQ in Eq. 2) of TMEs entering the NE-US using the local polynomial density estimation with the R package 'hdrcde' (Kim et al., 2011). Figure 9 shows that as the daily moisture release (ΔQ) by the TMEs increases, the daily precipitation increases with a shift in the conditional distribution that is marked beyond a threshold of ΔQ of about 3500 g kg-1. This observation based on data pooled over the whole year motivates a seasonal analysis of the association between extreme TMEs and extreme precipitation for different seasons, which is illustrated in Figure 10. The boxplot of the moisture releases (ΔQ) from the TMEs to NE-US are significantly different (p-value 0.01 to 0.001) with two-sample Kolmogorov-Smirnov test) given extreme or non-extreme rainfall states for all the four seasons. An extreme rainfall event is defined as one exceeding the 99th percentile of daily rainfall (including days with no or trace rain) in that season, e.g., an extreme rainfall event in DJF must exceed the 99th percentile of daily rainfall amounts in all the Dec, Jan and Feb over the 22 years. The seasonal 99th percentile

thresholds are 12.7cm (DJF), 12.2cm (MAM), 11.4cm (JJA) and 15.0cm (SON). For all the four seasons, non-extreme rainfall days have their average moisture releases from TMEs around 0 g kg-1 with thin, long tails.

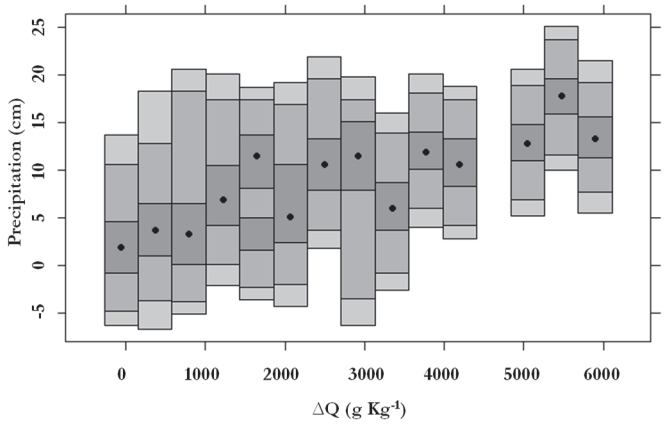

Figure 9. Kernel conditional density of daily precipitation given total changes of specific humidity of TMEs entered NE-US from 1989 – 2010, estimated using local polynomial. ΔQ is calculated by Eq.1

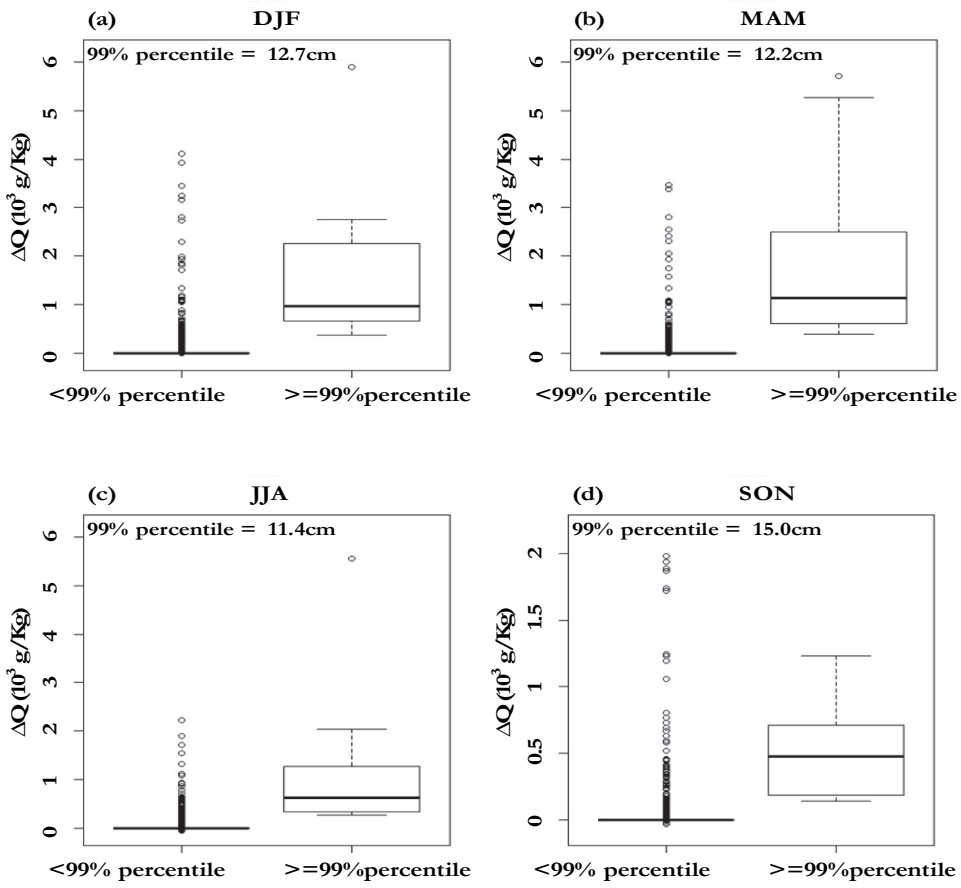

Figure 10. Boxplots of the moisture releases (ΔQ, unit: g kg^{-1}) from the TMEs to NE-US for each season given concurrent extreme: exceeding seasonal 99th percentile threshold, left in each panel or non-extreme rainfall states, on the right of each panel. The seasonal 99th percentile thresholds are (a) DJF, 12.7cm; (b) MAM, 12.2cm; (c) JJA, 11.4cm and (d) SON, 15.0cm

We further examined the ENSO influence on the extreme rainfall events occurrence. The number of extreme events fall into each ENSO episode is tabulated in Table 2. Summarizing on a monthly basis for the 22 years, there are 36 extreme events in La Niña years, with 16 events in El Niño years out of 83 total events at the 99th of daily rainfall by season. Extremes in June have 5 out of total 7 in La Niña years, against 0 in El Niño years.

March, April and September also have similar observations. However, due to the limitation of the sample size, the statistical significance is weak (e.g., p=0.18 for June, even though we have 0 El Niño and 5 La Niña cases).

On a monthly basis, the numbers of TMEs entering the NE-US for extreme precipitation events is consistently larger than those for non-extreme events. The definition of monthly extreme rainfall events is the same as that for seasonal extreme events except that the 99th percentile thresholds are taken for each month. Table 3 provides the ratio of the average number of TMEs tracks entering NE-US from each source in every month. The ratio is the average over all extreme events divided by the average over all non-extreme events. As the year-around major source, GP shows consistent intensification of TMEs entrance on extreme rainy days. The average TMEs from GP on extreme rainy days are 4 to 7 times of the average on non-extreme days. The difference of TMEs counts for days in the above and below 99th percentile rainfall categories is statistically significant with a p-value of less than 0.001 for the null hypothesis of no difference. The second major source, GS shows year-around intensification of TMEs entrance except for July when the ratio is close to 1. The intensification is stronger in GS than GP due to the fact that the average TMEs from GS on non-extreme rainfall days are less than those from GP, but their average number of TMEs tracks on extreme rainy days are comparable. This suggests that for extreme rainfall events, GP and GS are both important. Both PE and WP are active contributors to NE-US from Oct to Apr (Figure 6 (c) & (d)) and contribute very little from May to Sep. The average TMEs entrance from PE and WP are less than 3 for non-extreme rainy days from May to Sep/Aug, and hence the corresponding entries in Table 3 are left blank. Although the ratios for PE in Mar and for WP in April are large, their contributions to extreme rainfall events are less than those from GP and GS.

Table 2. ENSO influence on the number extreme rainfall events, i.e. exceeding the 99th percentile threshold of that calendar month over the 22 years' data period

Month	99th Rainfall (cm)	El Niño	La Niña	Neutral
Jan	14.7	1	3	3
Feb	11.3	3	1	2
Mar	12.8	1	5	1
Apr	12.9	1	4	2
May	11.1	2	3	2
Jun	11.3	0	5	2
Jul	11.7	2	1	4
Aug	11.0	1	2	4
Sep	14.5	1	4	2
Oct	15.0	3	2	2
Nov	16.0	0	3	4
Dec	13.0	1	3	3
No. of Years		5	8	9

Table 3. The ratio of average TMEs tracks entering NE-US from each source: extreme rainfall events over non-extreme rainfall events; extreme rainfall events are defined as the ones exceeding the 99th percentile of daily rainfall for each month; some entries are blank because the average number of tracks are less than 3 for non-extreme events; the differences between the two samples (i.e. Extreme rainfall case vs. Non-extreme rainfall case) are statistically significant (P-value < 0.001 with t-test) for the white entries; insignificant months are marked grey

Month	GP	GS	PE	WP
Jan	4.08	9.39	2.80	6.46
Feb	6.40	7.08	8.60	8.92
Mar	4.02	7.72	10.67	9.85
Apr	4.00	8.33	2.94	25.67
May	3.30	8.91		
Jun	4.19	5.69		
Jul	3.76	0.89		
Aug	6.48	5.16		
Sep	6.20	8.18		2.75
Oct	4.51	5.88	5.69	12.78

Nov	3.50	4.52	7.06	9.54
Dec	4.92	8.87	4.91	11.74

7. Summary and Discussion

The key findings of the paper are summarized as follows:

1. The NE-US floods in the four seasons are closely related to TMEs as evidenced by the historical flood events (Figure 2).
2. The four major moisture sources of TMEs account for approximately 85% of all the TMEs entering the NE-US, by calculating the ratio of TMEs born in these four major moisture sources over all TMEs that entering the study region (given in Table B.1 that $36694/43256 \approx 85\%$). The birth processes in the four source regions are relatively independent, except for moderate association between GP and GS in some months. They all have strong seasonality and interannual variation, which determine their contributions to the NE-US. Their overall contributions can be ordered as GP>GS>PE>WP (by comparing the last row in Table B.1), with GP and GS as the year-around sources, and PE active in winter, and WP as the smallest contributor.
3. Depending on the month, some of the interannual variations of TMEs birth are associated with ENSO phases (Figure 3). Since GP is the dominant contributor and year-around source, the influence of ENSO on GP-TMEs' birth affects the TMEs' entrance to NE-US. The intensification of TMEs born between October and January during El Niño suggests that more TMEs could potentially enter NE-US under the influence of ENSO warm phase, which may result in more moisture release and precipitation. Since the ENSO warm phase also leads to an intensification of the GS birth process, the two major sources would contribute more TMEs potentially, when the steering mechanisms cooperated in the convergence of tracks to the NE-US. The GP and GS TMEs track entrances are highly correlated over several months, and this may reflect the common influences on the birth and steering processes.
4. The seasonal and interannual variations in atmospheric circulation patterns also play an important role in determining the TMEs' entrance to NE-US. Aggregating cross the four major sources, the annual maximum of TMEs entrance occurs in June and the minimum occurs in winter (Figure 5 (a)). The order of importance of the four sources is consistent with observations in the floods examples in the beginning: GP>GS>PE>WP (Figure 5 (b)). However different from the ENSO effect on the birth process, no significant difference was observed among different ENSO episodes for the entrance given a birth source, suggesting the ENSO has more influence on birth than steering mechanism. The composite SLPa of active TMEs days and inactive TMEs days suggests that low wave number patterns of atmospheric circulation mark the anomalous transport (Figure 7 and Figure 8). Depending on the calendar month, these patterns are not always symmetric for active vs inactive TMEs periods suggesting that the circulation processes driving the TMEs to the NE-US are nonlinear.
5. The number of tracks entering and the associated moisture release are highly correlated, with correlation 0.88 (p-value $< 10^{-4}$). This translates into a strong influence of active TMEs periods on the occurrence of extreme rainfall. The distribution of TMEs for extreme rainfall events (>the 99th percentile of daily rainfall) is significantly different from the one given non-extreme events (Figure 10), suggesting the important role of TMEs in determining extreme precipitation. This argument carries forward into shifts in extreme rainfall event occurrence across different ENSO phases as they influence the TMEs birth and steering.

The study of atmospheric rivers as an influence on floods induced by extreme precipitation has significantly enhanced the interaction between hydrologists and climate scientists towards an improved understanding of the synoptic and climatological factors that govern such phenomena. The NE-US has not been the target of many of these investigations, partly because of the way atmospheric rivers have been defined, although some debate on the definition still remains. The Knippertz and Wernli work established the broader role of tropical moisture exports in the climatology of mid-latitude precipitation, and provided a data base that allows a consistent exploration of the Lagrangian transport of moisture from the tropics to the mid-latitudes. Our initial work on a flood over Western France in 1995 revealed that at synoptic scales systematic organization of moisture as reflected in the data not including 1995 could be identified by a simple statistical model and used effectively for an out of sample prediction of the extreme precipitation in January 1995 that led to the flood event. Several of the moisture tracks associated with that flood event also had a moisture release over the NE-US, stimulating the work reported in this paper. Here, we explore climatological aspects of the links between TMEs birth, steering,

moisture release and extreme precipitation, providing the first such chronology of the year-round links between these factors, as well as the potential links to ENSO.

Given the short record of TMEs available to us, a structured exploration of interannual variability and an association with ENSO and lower frequency phenomenon was not possible. However, we expect to extend the work reported here in multiple directions. First, we expect that a national analysis will be much more informative as to the spatial and temporal shifts in TMEs' influence on extreme precipitation by season and as driven by identified low frequency climate mechanisms. Developing a formal spatiotemporal model that considers the connectivity across such a source-destination network and its modulation by atmospheric and ocean circulation precursors is a challenge worthy of pursuit. As we develop such a model, we expect to utilize longer atmospheric-reanalysis data and to develop a longer TMEs record from it using LAGRANTO as was done by Knippertz and Wernli using the ERA-Interim data. Such a development may provide a much better empirical understanding of extreme precipitation dynamics across the USA, and thus provide an important diagnostic tool for the performance of climate models for seasonal forecasting or for climate change simulations. The nationwide study will also consider the recycling of moisture suggested by Dirmeyer et al. (2009).

Acknowledgements

The floods record is available at the website of the Dartmouth Flood Observatory (DFO: http://floodobservatory.colorado.edu/). The TMEs data is provided by P. Knippertz, documented in *Knippertz and Wernli* (2010) and *Knippertz et al.* (2013). The NCEP/NCAR Reanalysis dataset is provided by the NOAA/OAR/ESRL PSD, Boulder, Colorado, USA, from their Web site at http://www.esrl.noaa.gov/psd/. The Oceanic Niño Index (ONI) is provided by NOAA/National Weather Service, NOAA Center for Weather and Climate Prediction, Climate Prediction Center, from their website at http://www.cpc.ncep.noaa.gov/. The publication is financially supported by the Hong Kong University of Science and Technology start-up fund (R9392).

References

Bao, J. W., Michelson, S. A., Neiman, P. J., Ralph, F. M., & Wilczak, J. M. (2006). Interpretation of Enhanced Integrated Water Vapor Bands Associated with Extratropical Cyclones: Their Formation and Connection to Tropical Moisture. *Mon. Weather Rev.*, *134*, 1063–1080. https://doi.org/10.1175/MWR3123.1

Cioffi, F., Lall, U., Rus, E., & Krishnamurthy, C. K. B. (2015a). Space-time structure of extreme precipitation in Europe over the last century. *Int. J. Climatol.*, *35,* 1749–1760. https://doi.org/10.1002/joc.4116

Dacre, H. F., & Coauthors (2015) How Do Atmospheric Rivers Form? *Bull. Am. Meteorol. Soc.*, *96*, 1243–1255, https://doi.org/10.1175/BAMS-D-14-00031.1

Dee, D. P., & Coauthors, 2011: The ERA-Interim reanalysis: configuration and performance of the data assimilation system. *Q. J. R. Meteorol. Soc.*, *137*, 553–597. https://doi.org/10.1002/qj.828

Dettinger, M. (2011). Climate Change, Atmospheric Rivers, and Floods in California - A Multimodel Analysis of Storm Frequency and Magnitude Changes1. *JAWRA J. Am. Water Resour. Assoc., 47*, 514–523, https://doi.org/10.1111/j.1752-1688.2011.00546.x

Dettinger, M. D., Ralph, F. M., Das, T., Neiman, P. J., & Cayan, D. R. (2011). Atmospheric Rivers, Floods and the Water Resources of California. *Water*, *3*, 445–478. https://doi.org/10.3390/w3020445

Dirmeyer, P. A., Brubaker, K. L., & DelSole, T. (2009). Import and export of atmospheric water vapor between nations. *J. Hydrol.*, *365,* 11–22. https://doi.org/10.1016/j.jhydrol.2008.11.016

Francesco, C., Upmanu, L., Ester, R., & Chandra, K. B. K. (2015b). Space-time structure of extreme precipitation in Europe over the last century. *Int. J. Climatol.*, *35*, 1749–1760. https://doi.org/10.1002/joc.4116

Heini, W., & Davies, H. C. (1997). A Lagrangian-based analysis of extratropical cyclones. I: The method and some applications. *Q. J. R. Meteorol. Soc.*, *123,* 467–489. https://doi.org/10.1256/smsqj.53810

Higgins, R. W., Schemm, J. K. E., Shi, W., & Leetmaa, A. (2000). Extreme Precipitation Events in the Western United States Related to Tropical Forcing. *J. Clim.*, *13,* 793–820, https://doi.org/10.1175/1520-0442(2000)013<0793:EPEITW>2.0.CO;2

Jain, S., Lall, U., & Mann, M. E. (1999). Seasonality and Interannual Variations of Northern Hemisphere Temperature: Equator-to-Pole Gradient and Ocean–Land Contrast. *J. Clim.*, *12,* 1086–1100, https://doi.org/10.1175/1520-0442(1999)012<1086:SAIVON>2.0.CO;2

Jeon, S., Byna, S., Gu, J., Collins, W. D., & Wehner, M. F. (2015). Characterization of extreme precipitation within atmospheric river events over California. *Adv. Stat. Clim. Meteorol. Ocean.*, *1*, 45–57. https://doi.org/10.5194/ascmo-1-45-2015

Kalnay, E., & Coauthors (1996). The NCEP/NCAR 40-year reanalysis project. *Bull. Am. Meteorol. Soc.*, *77,* 437–471. https://doi.org/10.1175/1520-0477(1996)077<0437:TNYRP>2.0.CO;2

Karamperidou, C., Cioffi, F., & Lall, U. (2012). Surface Temperature Gradients as Diagnostic Indicators of Midlatitude Circulation Dynamics. *J. Clim.*, *25*, 4154–4171. https://doi.org/10.1175/JCLI-D-11-00067.1

Kim, J. H., Fraser, I., & Hyndman, R. J. (2011). Improved interval estimation of long run response from a dynamic linear model: A highest density region approach. *Comput. Stat. Data Anal., 55*, 2477–2489, https://doi.org/10.1016/j.csda.2011.03.003

Knippertz, P., & Martin, J. E. (2007). A Pacific Moisture Conveyor Belt and Its Relationship to a Significant Precipitation Event in the Semiarid Southwestern United States. *Weather Forecast.*, *22*, 125–144, https://doi.org/10.1175/WAF963.1

Laing, A. G., & Fritsch, J. M. (1997). The global population of mesoscale convective complexes. *Q. J. R. Meteorol. Soc.*, *123*, 389–405. https://doi.org/10.1002/qj.49712353807

Lavers, D. A., Allan, R. P., Villarini, G., Lloyd-Hughes, B., Brayshaw, D. J., & Wade, A. J. (2013). Future changes in atmospheric rivers and their implications for winter flooding in Britain. *Environ. Res. Lett.*, *8,* 34010, https://doi.org/10.1088/1748-9326/8/3/034010

Lavers, D. A., Allan, R. P., Wood, E. F., Villarini, G., Brayshaw, D. J., & Wade, A. J. (2011). Winter floods in Britain are connected to atmospheric rivers. *Geophys. Res. Lett.*, *38,* L23803. https://doi.org/10.1029/2011GL049783

Lavers, D. A., Waliser, D. E., Ralph, F. M., & Dettinger, M. D. (2016). Predictability of horizontal water vapor transport relative to precipitation: Enhancing situational awareness for forecasting western U.S. extreme precipitation and flooding. *Geophys. Res. Lett.*, *43,* 2275–2282. https://doi.org/10.1002/2016GL067765

Leung, L. R., & Qian, Y. (2009). Atmospheric rivers induced heavy precipitation and flooding in the western U.S. simulated by the WRF regional climate model. *Geophys. Res. Lett.*, *36,* L03820, https://doi.org/10.1029/2008GL036445

Lorenz, E. N. (1984). Irregularity: a fundamental property of the atmosphere. *Tellus A*, *36A,* 98–110, https://doi.org/10.1111/j.1600-0870.1984.tb00230.x

Lu, M., Lall, U., Schwartz, A., & Kwon, H. (2013). Precipitation predictability associated with tropical moisture exports and circulation patterns for a major flood in france in 1995. *Water Resour. Res.*, *49*, 6381–6392, https://doi.org/10.1002/wrcr.20512

Nakamura, J., Lall, U., Kushnir, Y., Robertson, A. W., & Seager, R. (2013). Dynamical Structure of Extreme Floods in the US Midwest and the United Kingdom. *J. Hydrometeorol.*, *14*, 485–504, https://doi.org/10.1175/JHM-D-12-059.1

Neiman, P. J., Ralph, F. M., Wick, G. A., Kuo, Y. H., Wee, T. K., Ma, Z., Taylor, G. H., & Dettinger, M. D. (2008). Diagnosis of an Intense Atmospheric River Impacting the Pacific Northwest: Storm Summary and Offshore Vertical Structure Observed with COSMIC Satellite Retrievals. *Mon. Weather Rev.*, *136,* 4398–4420, https://doi.org/10.1175/2008MWR2550.1

Peter, K., & Heini W. (2010). A Lagrangian Climatology of Tropical Moisture Exports to the Northern Hemispheric Extratropics. *J. Clim.*, *23*, 987–1003. https://doi.org/10.1175/2009JCLI3333.1

Peter, K., Heini W., & Gläser, G. (2013). A Global Climatology of Tropical Moisture Exports. *J. Clim.*, *26*, 3031–3045. https://doi.org/10.1175/JCLI-D-12-00401.1

Ralph, F. M., & Dettinger, M. D. (2011). Storms, floods, and the science of atmospheric rivers. *Eos, Trans. Am. Geophys. Union*, *92*, 265. https://doi.org/10.1029/2011EO320001

Ralph, F. M., Neiman, P. J., & Wick, G. A. (2004). Satellite and CALJET Aircraft Observations of Atmospheric Rivers over the Eastern North Pacific Ocean during the Winter of 1997/98. *Mon. Weather Rev.*, *132*, 1721–1745, https://doi.org/10.1175/1520-0493(2004)132<1721:SACAOO>2.0.CO;2

Ralph, F. M., Neiman, P. J., Wick, G. A., Gutman, S. I., Dettinger, M. D., Cayan, D. R., & White, A. B. (2006). Flooding on California's Russian River: Role of atmospheric rivers. *Geophys. Res. Lett.*, *33*, L13801,

https://doi.org/10.1029/2006GL026689

Ryoo, J. M., Waliser, D. E., & Fetzer, E. J. (2011). Trajectory analysis on the origin of air mass and moisture associated with Atmospheric Rivers over the west coast of the United States. *Atmos. Chem. Phys. Discuss.*, *11,* 11109–11142. https://doi.org/10.5194/acpd-11-11109-2011

Screen, J. A., & Simmonds, I. (2014). Amplified mid-latitude planetary waves favour particular regional weather extremes. *Nat. Clim. Chang.*, *4*, 704–709. https://doi.org/10.1038/nclimate2271

Smith, T. M., Reynolds, R. W., Peterson, T. C., & Lawrimore, J. (2008). Improvements to NOAA's Historical Merged Land–Ocean Surface Temperature Analysis (1880–2006). *J. Clim.*, *21,* 2283–2296, https://doi.org/10.1175/2007JCLI2100.1

Wernli, H. (1997). A Lagrangian-based analysis of extratropical cyclones. II: A detailed case-study. *Q. J. R. Meteorol. Soc.*, *123*, 1677–1706. Retrieved from http://cat.inist.fr/?aModele=afficheN&cpsidt=2773474

Zhu, Y., & Newell, R. E. (1994). Atmospheric rivers and bombs. *Geophys. Res. Lett.*, *21,* 1999–2002. https://doi.org/10.1029/94GL01710

Zhu, Y., & Newell, R. E. (1998). A Proposed Algorithm for Moisture Fluxes from Atmospheric Rivers. *Mon. Weather Rev.*, *126*, 725–735. https://doi.org/10.1175/1520-0493(1998)126<0725:APAFMF>2.0.CO;2

Appendix A

Enlarged figures for Figure 2

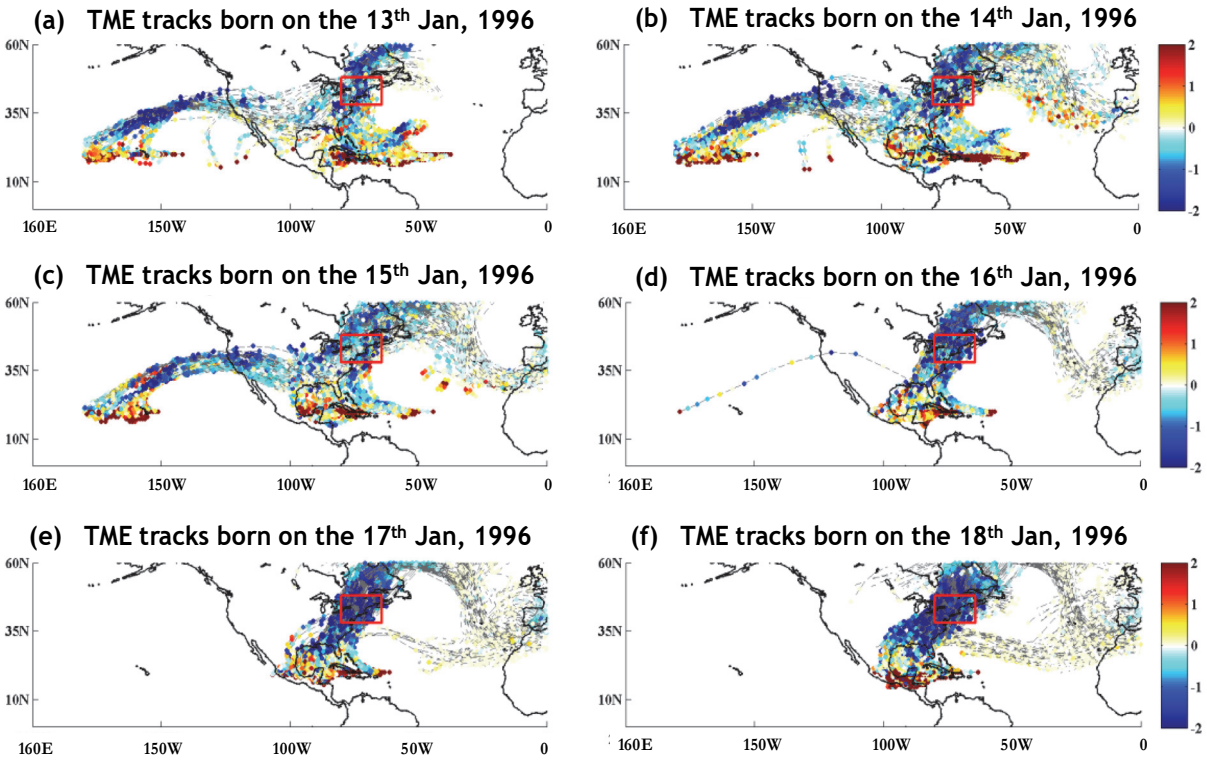

Figure A.1 Enlarged figure for Figure 2 (a) - (f): DJF Flood: TMEs tracks that born between the 13th and the 18th Jan in 1996, two successive flood events occurred, one started on the 15th in New York, Pennsylvania, Ohio, West Virginia, New Jersey; the other started 4 days later in Chateauguay, Quebec

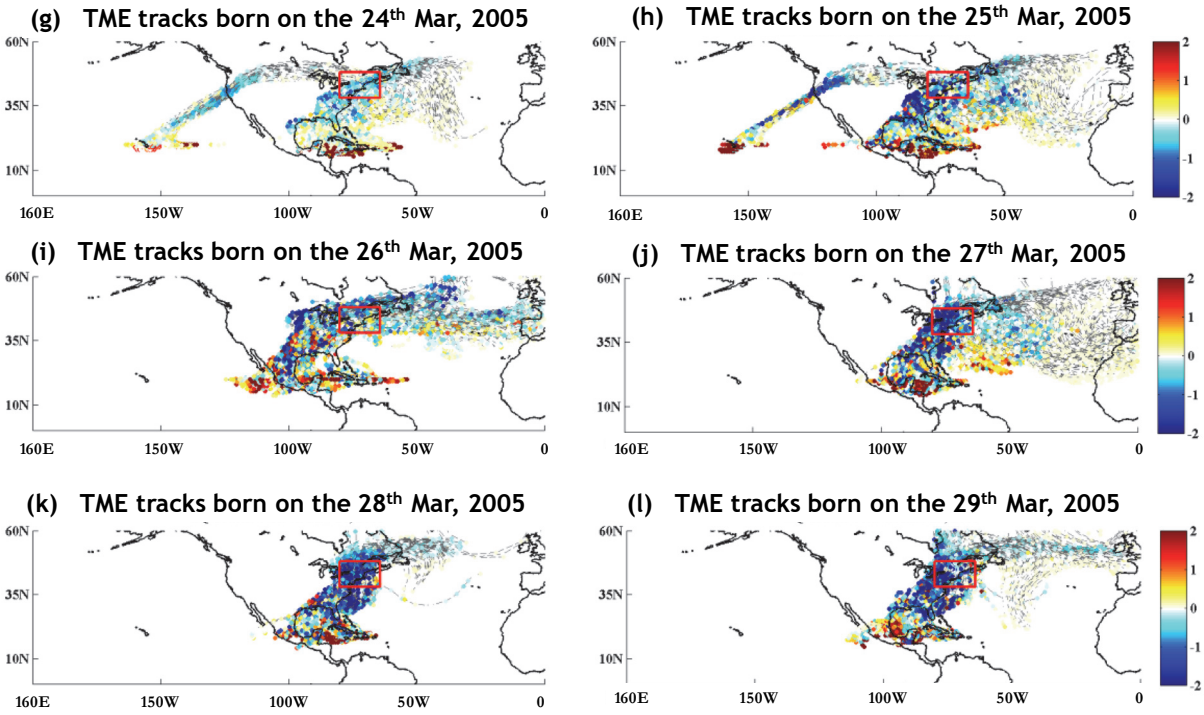

Figure A.2. Enlarged figure for Figure 2 (g) - (l): MAM flood: TMEs tracks that born between the 24th and the 29th Mar in 2005; broad area including New York, New Jersey, Delaware had flood starting on the 1st of April

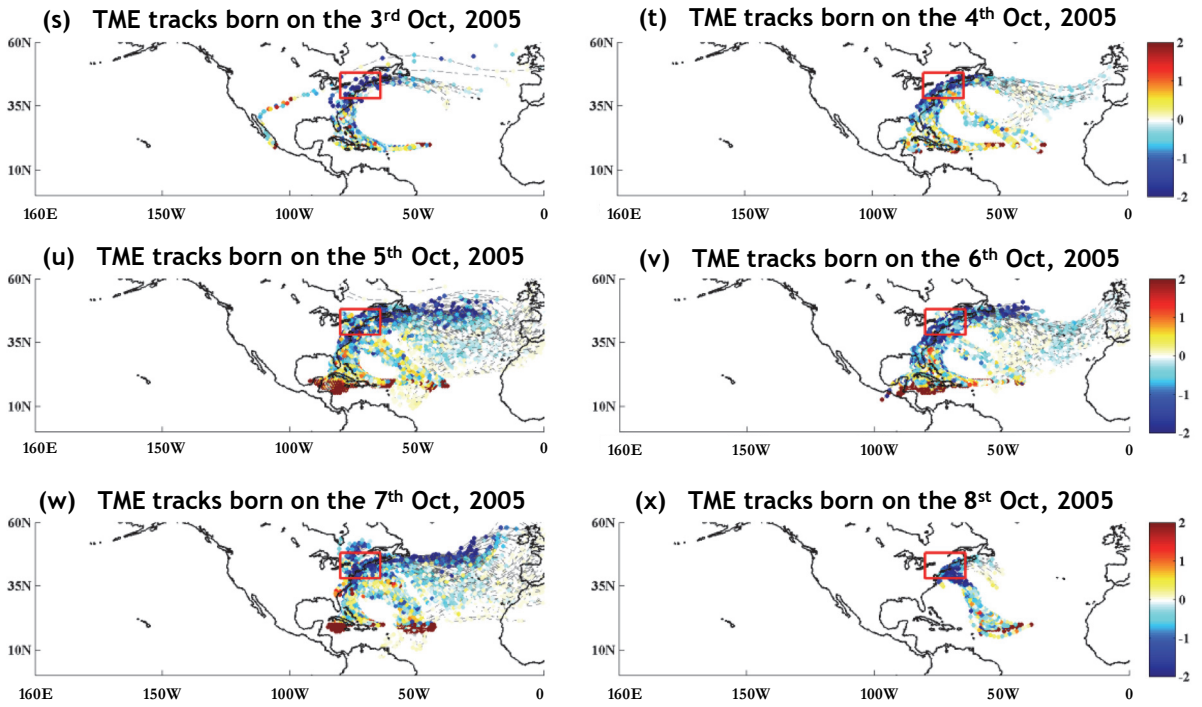

Figure A.3. Enlarged figure for Figure 2 (m) – (r): JJA flood: TMEs tracks that born between the 17th and the 22nd Jul in 1998; heavy rainfall induced flood event in Green Mountain to Bradford, Vermont and New Hampshire

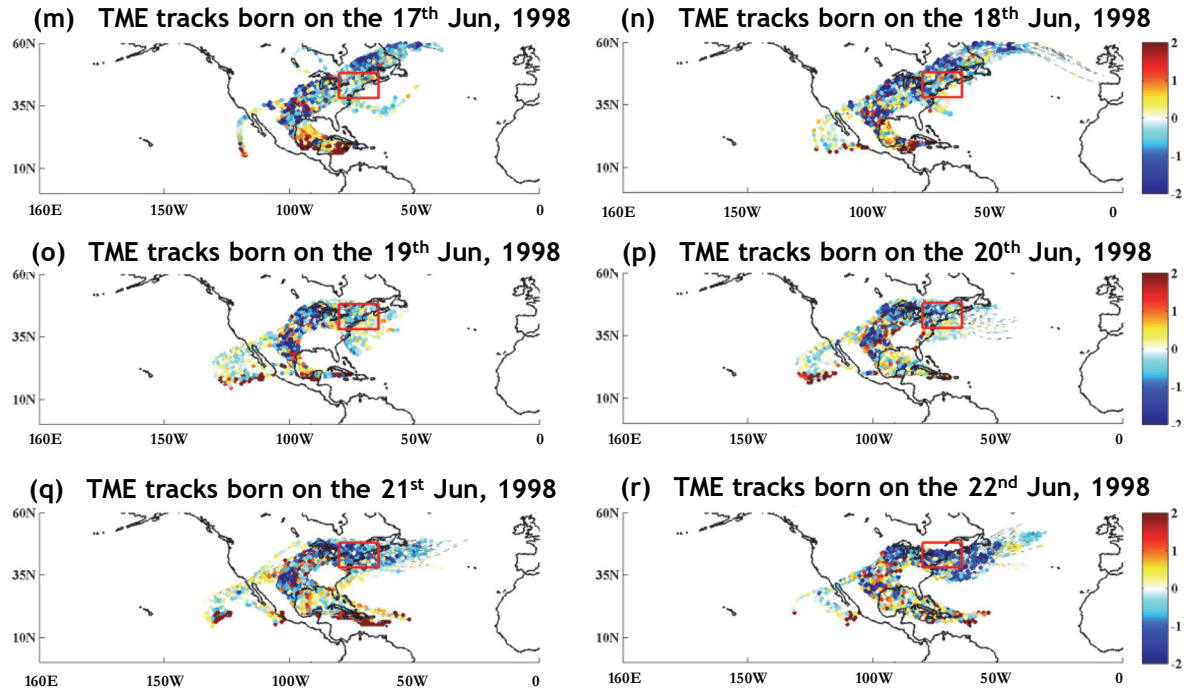

Figure A.4. Enlarged figure for Figure 2 (s) – (x) SON flood: TMEs tracks that born between the 3rd and 8th Oct in 2005 associated with 10 days flooding from the 8th to the 17th of Oct in Southwest New Hampshire, Vermont, New Jersey and Connecticut

Appendix B

Supplementary tables

Table B.1. Conditional probability of TMEs sources given the tracks entering N.E. US region [39°N – 48°N, 66°W-82°W] in each month through a year, the conditional probability is averaged over 22 years of data, from 1989 to 2010. The last two columns correspond to number of tracks from the four major sources and number of tracks from all sources including the four and anywhere outside these

	Conditional probability of TMEs sources given tracks entered NE: P(Source|NE)					
Month	**P(GP|NE)**	**P(GS|NE)**	**P(PE|NE)**	**P(WP|NE)**	**#Tracks born in (PE,WP,GS,GP) & entered NE**	**#Tracks**
Jan	0.484	0.072	0.211	0.027	3590	4622
Feb	0.513	0.083	0.161	0.041	3208	3933
Mar	0.655	0.071	0.107	0.031	3758	4358
Apr	0.745	0.063	0.047	0.028	3060	3488
May	0.768	0.091	0.040	0.023	2887	3118
Jun	0.787	0.132	0.003	0.017	3757	3956
Jul	0.781	0.202	0.000	0.003	2631	2682
Aug	0.677	0.277	0.001	0.019	2114	2171
Sep	0.599	0.242	0.020	0.061	2764	2969
Oct	0.556	0.132	0.083	0.032	2485	3004
Nov	0.454	0.068	0.173	0.034	2859	3861
Dec	0.461	0.068	0.180	0.042	3582	5095
Annual total #tracks	26670	4974	3920	1130	36694	43256

Table B.2. Conditional probability of tracks entering the N.E. US [39°N – 48°N, 66°W-82°W] region, given tracks born in the four major sources in each month through a year, the conditional probability is averaged over 22 years of data, from 1989 to 2010

	Conditional Probability of tracks entered NE given born in the sources: P(NE|Source)					
Month	**P(NE|GP)**	**P(NE|GS)**	**P(NE|PE)**	**P(NE|WP)**	**#Tracks born in (PE,WP,GS,GP) & entered NE**	**#Tracks born in (PE,WP,GS,GP)**
Jan	0.392	0.119	0.178	0.037	3590	18906
Feb	0.349	0.098	0.117	0.036	3208	18510
Mar	0.469	0.118	0.085	0.015	3758	21237
Apr	0.496	0.085	0.033	0.011	3060	21526
May	0.368	0.080	0.032	0.006	2887	28879
Jun	0.382	0.131	0.001	0.004	3757	36917
Jul	0.339	0.154	0.000	0.000	2631	32381
Aug	0.373	0.225	0.001	0.002	2114	24895
Sep	0.465	0.213	0.016	0.009	2764	23217
Oct	0.470	0.094	0.084	0.011	2485	19714
Nov	0.513	0.109	0.313	0.022	2859	14215
Dec	0.422	0.116	0.282	0.044	3582	17569
Annual total #tracks	26670	4974	3920	1130	36694	277965